catalysts

Supplementary Information

The Tailored Surface Oxygen Vacancies and Reduced Optical Band Gap of NiO During the Development of NiO@Polyaniline Hybrid Materials for the Efficient Asymmetric and Oxygen Evolution Reaction Applications

Fida Hussain [1], Wanhinyal Dars [1], Rabia Kanwal [1], Jethanand Parmar [1], Ghansham Das [1], Ahmed Raza [1], Haresh Kumar [1], Rameez Mangi [1], Masroor Ali Bhellar [1], Ambedker Meghwar [1], Kashif Ali [1], Aneela Tahira [2], Muhammad Ali Bhatti [3], Elmuez Dawi [4,*], Rafat M. Ibrahim [5], Brigitte Vigolo [6] and Zafar Hussain Ibupoto [1,*]

[1] Institute of Chemistry, University of Sindh, Jamshoro 76080, Sindh, Pakistan; wanhinyald@gmail.com (W.D.)
[2] Institute of Chemistry, Shah Abdul Latif University, Khairpur Mirs 66020, Sindh, Pakistan
[3] Centre for Environmental Sciences, University of Sindh, Jamshoro 76080, Sindh, Pakistan
[4] Mathematics and Science Department, College of Humanities and Sciences, Ajman University, Ajman P.O. Box 346, United Arab Emirates
[5] Physics Department, Faculty of Science, Taibah University, Al-Madaina Al Munawarah 42353, Saudi Arabia; rtum@taibahu.edu.sa
[6] CNRS, IJL, University de Lorraine, F-54000 Nancy, France; brigitte.vigolo@univ-lorraine.fr
* Correspondence: e.dawi@ajman.ac.ae (E.D.); zaffar.ibhupoto@usindh.edu.pk (Z.H.I.)

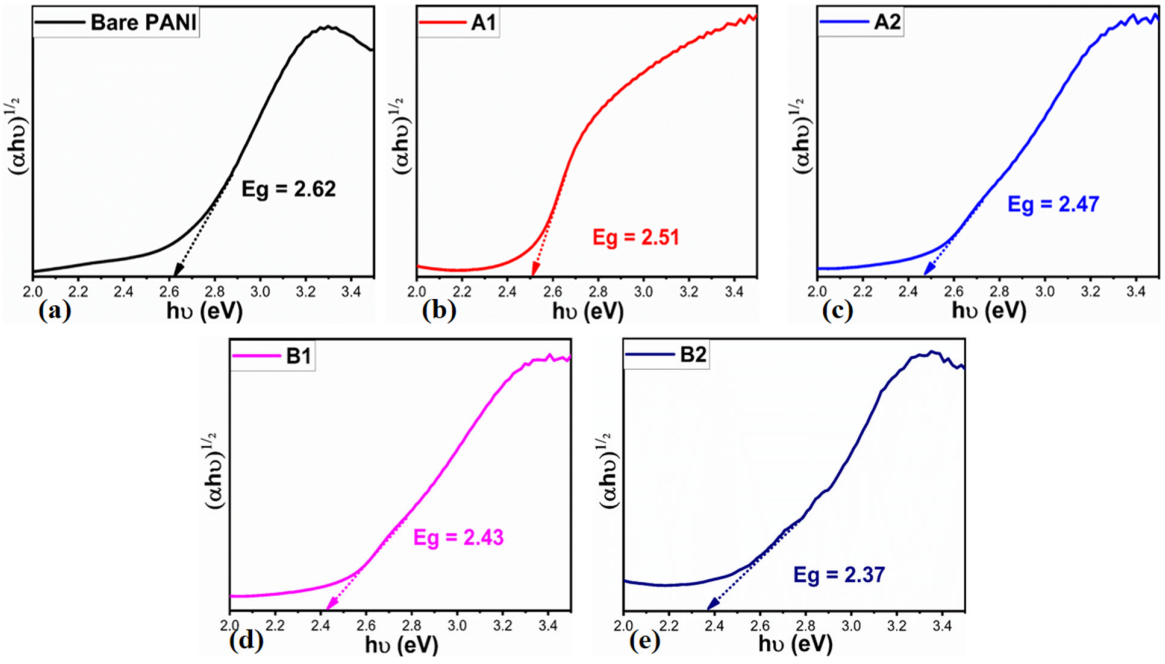


Figure (S1): Tauc,s plots of bare PANI, A1, A2, B1 and B2 for the estimation of optical band gap

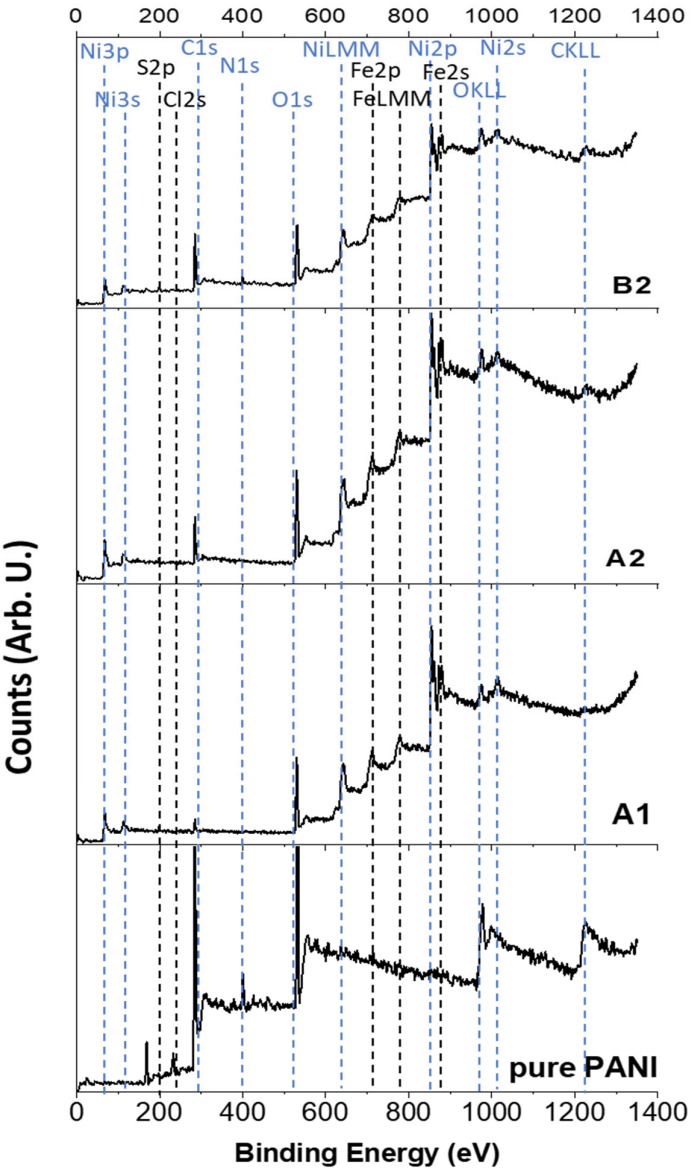


Figure (S2): XPS survey spectra of Pure PANI, pure NiO (A1) and A2 and B2 composites

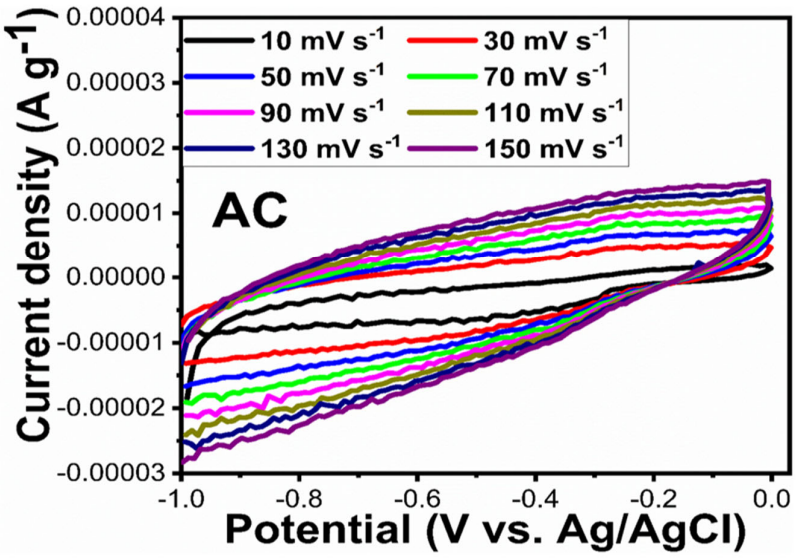


Figure (S3): CV curves at different scan rates. Activated carbon in 3 M KOH solution.

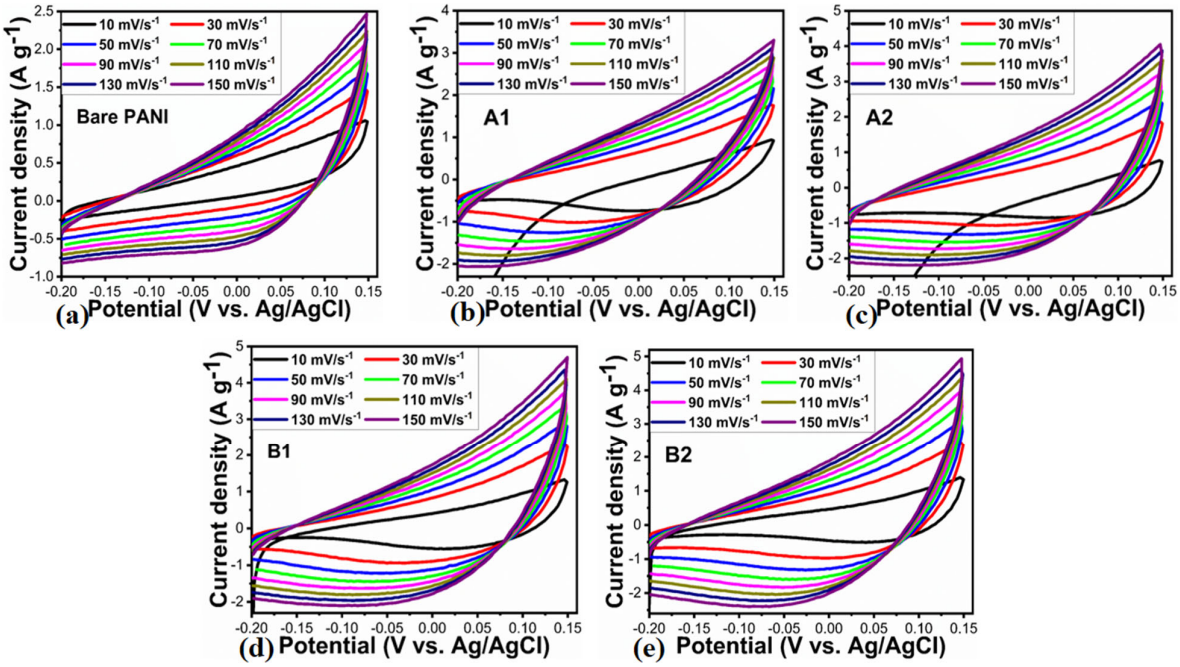


Figure (S4): (a-e) CV curves in non-faradic region of bare PANI, A1, A2, and B1 and B2 materials at various scan rates in 3 M KOH electrolytic solution for the estimation of ECSA values.

Table (S1): Summarized electrochemical performance of various electrode materials such as bare nickel foam/PANI, A1, A2, and B2, B2.

Material	Specific Capacitance (Fg^{-1})	Current Density (Ag^{-1})	Operating Voltage window
Bare NF	47.36	2	0-0.4 V
	43.73	3	0-0.4 V
	36.83	4	0-0.4 V
	30.69	5	0-0.4 V
	12.79	10	0-0.4 V
Bare Polyaniline	70.08	2	0-0.4 V
	61.38	3	0-0.4 V
	54.22	4	0-0.4 V
	42.20	5	0-0.4 V
	28.13	10	0-0.4 V
A1	489.95	2	0-0.4 V
	322.61	3	0-0.4 V
	255.28	4	0-0.4 V
	204.77	5	0-0.4 V
	60.30	10	0-0.4 V
A2	525.25	2	0-0.4 V
	415.91	3	0-0.4 V
	297.23	4	0-0.4 V
	227.39	5	0-0.4 V
	77.69	10	0-0.4 V
B1	958.19	2	0-0.4 V
	802.76	3	0-0.4 V
	411.56	4	0-0.4 V
	310.30	5	0-0.4 V
	278.89	10	0-0.4 V
B2	1655.78	2	0-0.4 V
	1062.66	3	0-0.4 V
	723.27	4	0-0.4 V
	367.01	5	0-0.4 V
	342.71	10	0-0.4 V

Table (S2): Comparative study of B2 as anode material for ASC with recently reported ASC device.

Material	Specific Capacitance (Fg^{-1})	Energy Density (Wh kg^{-1})	Power Density (W kg^{-1})	Operating Voltage window	Reference
$NiCu(OH)_2CO_3$//AC	476 F g^{-1}	48.55 Wh kg^{-1}	541 W kg^{-1}	0.6 V	1
RuO_2//h-WO_3	47.59 F g^{-1}	16.92 W h kg^{-1}	540 W/kg	1.6 V	2
Co1Ni1//AC	106	42.5 Wh kg^{-1}	849.7 W kg^{-1}	1.7 V	3
MnO_2/HCS-30//HCS	74.5 F g^{-1}	41.4 Wh kg^{-1}	-------	2.0 V	4
$NiCo_2O_4$@MnO_2// AC	112 F g^{-1}	58.9 W h kg^{-1}	400 W kg^{-1}	1.5 V	5
$MnCo_2O_{4.5}$-40 GQDs//rGO Ag QDs/	200 F g^{-1}	46 Wh kg^{-1}	66 W kg^{-1}	1.3 V	6
$NiMoO_4$//spore-derived AC	120.5 F g^{-1}	48.5 Wh kg^{-1}	212.5 kWh kg^{-1}	1.7 V	7
ZnO@CoS//AC	2438 mC cm^{-2}	45.2 Wh kg^{-1}	1039.1 W kg^{-1}	1.6V	8
$CoMoO_4$@CoS//AC	189.5 F g^{-1}	59.2 W h kg^{-1}	799.8 W kg^{-1}	1.7 V	9
NiCo–CH-180//AC	125	52	1500 W kg^{-1}	1.7 V	10
B2	**404.81**	**140.36**	**3160.00**	**1.6V**	**Here in**

1. Zheng X, Ye Y, Yang Q, Geng B, Zhang X, (2016) Ultrafine Nickel-Copper Carbonate Hydroxide Hierarchical Nanowire Networks for High-Performance Supercapacitor Electrodes, *Chem. Eng. J.*, 290**:** 353–360,
2. Ji SH, Chodankar NR, Kim DH, (2019. Aqueous asymmetric supercapacitor based on RuO2-WO3 electrodes. *Electrochimica Acta*, *325:*.134879.
3. Wang XL, Zhan GF, Nasser R, Jiang TT, Cao QW, Gong M, Li Y, Song JM, (2022) Controllable Synthesis of Co/Ni Basic Carbonate Composite *via* Regulating Co/Ni Ratio with Super Rate Performance for Asymmetric Solid-state Supercapacitor, *J. Alloys Compd.*, **906:** 164270,
4. Du W, Wang X, Zhan J, Sun X, Kang L, Jiang F, Zhang X, Shao Q, Dong M, Liu H, Murugadoss V, (2019) Biological cell template synthesis of nitrogen-doped porous hollow carbon spheres/MnO2 composites for high-performance asymmetric supercapacitors. *Electrochimica Acta*, *296:* 907-915.

5. Zhu D, Sun X, Yu J, Liu Q, Liu J, Chen R, Zhang H, Li R, Yu J, Wang J, (2019) Rationally designed CuCo2O4@ Ni (OH) 2 with 3D hierarchical core-shell structure for flexible energy storage. *Journal of colloid and interface science*, *557*: 76-83.
6. Zhang M, Liu W, Liang R, Tjandra R, Yu A, (2019) Graphene quantum dot induced tunable growth of nanostructured MnCo 2 O 4.5 composites for high-performance supercapacitors. *Sustainable Energy & Fuels*, *3*(9), pp.2499-2508.
7. Zhang X, Li Z, Yu Z, Wei L, Guo X, (2020) Mesoporous NiMoO4 microspheres decorated by Ag quantum dots as cathode material for asymmetric supercapacitors: enhanced interfacial conductivity and capacitive storage. *Applied Surface Science*, *505:* 144513.
8. Ding S, Li X, Jiang X, Hu Q, Yan Y, Zheng Q, Lin D, (2020) Core-shell nanostructured ZnO@ CoS arrays as advanced electrode materials for high-performance supercapacitors. *Electrochimica Acta*, *354:* 136711.
9. Xuan H, Li H, Yang J, Liang X, Xie Z, Han P, Wu Y, (2020) Rational design of hierarchical core-shell structured CoMoO4@ CoS composites on reduced graphene oxide for supercapacitors with enhanced electrochemical performance. *International Journal of Hydrogen Energy*, *45*(11): 6024-6035.
10. Kumar S, Satpathy BK, Pradhan D, (2024) Morphology-controlled synthesis of a NiCo-carbonate layered double hydroxide as an electrode material for solid-state asymmetric supercapacitors. *Materials Advances*, *5*(6): 2271-2284.

Table (S3): Comparative study of B2 as OER electrocatalytic material with recently reported electrocatalysts.

Material	**Tafel slope (mV/dec)**	**Overpotential (mV)**	**Current density (mA cm^{-2})**	Reference
NiSe–PANI	145.4	303	10	1
Mn3O4	85.6	370	10	2
NiO/MnO2@PANI	24	345	10	3
NiCo2O4/PANI	153	400	10	4
Co2.25Fe0.75O4	50	350	10	5
Fe90Nb10	50	340	10	6
Co/b-Mo2C@N-CNTs	67	356	10	7
B2	**34**	**320**	**10**	**Here in**

1. Liu PF, Zhang L, Zheng LR, Yang HG, (2018) Surface engineering of nickel selenide for an enhanced intrinsic overall water splitting ability, Materials Chemistry Frontiers, 2: 1725-1731.
2. Nagajyothi PC, Ramaraghavulu R, Munirathnam K, Yoo K, Shim J, (2021) One-pot hydrothermal synthesis: Enhanced MOR and OER performance using low-cost Mn3O4 electrocatalyst, International Journal of Hydrogen Energy, 46: 13946-13951.

3. He J, Wang M, Wang W, Miao R, Zhong W, Chen SY, Poges S, Jafari T, Song W, Liu J, Suib SL, (2017) Hierarchical mesoporous NiO/MnO2@ PANI core–shell microspheres, highly efficient and stable bifunctional electrocatalysts for oxygen evolution and reduction reactions. ACS Applied Materials & Interfaces. 13; 9 (49)42676-87.
4. Bhushan M, Mani M, Singh AK, Panda AB, Shahi VK, (2020) Self-standing polyaniline membrane containing quaternary ammonium groups loaded with hollow spherical NiCo2O4 electrocatalyst for alkaline water electrolyser, Journal of Materials Chemistry A, 8: 17089-17097.
5. Saddeler S, Bendt G, Salamon S, Haase FT, Landers J, Timoshenko J, Rettenmaier C, Jeon HS, Bergmann A, Wende H, Roldan Cuenya B, Schulz S, (2021) Influence of the cobalt content in cobalt iron oxides on the electrocatalytic OER activity, Journal of Materials Chemistry A, (2021).
6. Wang C, Wang R, Peng Y, Chen J, Chen Z, Yin H, Li J, (2020) Nb-incorporated Fe (oxy)hydroxide derived from structural transformation for efficient oxygen evolution electrocatalysis, Journal of Materials Chemistry A, 8: 24598-24607.
7. Ouyang T, Ye YQ, Wu CY, Xiao K, Liu ZQ, (2019) Heterostructures Composed of N-Doped Carbon Nanotubes Encapsulating Cobalt and β-Mo2C Nanoparticles as Bifunctional Electrodes for Water Splitting, Angewandte Chemie International Edition, 58: 4923-4928.